Journal of Mechatronics, Electrical Power, and Vehicular Technology 15 (2024) 220-229

Journal of Mechatronics, Electrical Power, and Vehicular Technology

e-ISSN: 2088-6985
p-ISSN: 2087-3379

mev.brin.go.id

Design of switched reluctance motor as actuator in an end-effector-based wrist rehabilitation robot

Budi Azhari [a, *], Muhammad Fathul Hikmawan [a], Aditya Sukma Nugraha [a], Edwar Yazid [a], Aji Nasirohman Pakha [b], Catur Hilman Adritya Haryo Bhakti Baskoro [a], Rahmat [a], Mohamad Luthfi Ramadiansyah [a, c]

[a] *Research Center for Smart Mechatronics, National Research and Innovation Agency (BRIN)*
Kawasan Sains dan Teknologi (KST) Samaun Samadikun, Jalan Sangkuriang, Bandung, 40135, Indonesia

[b] *National Cheng Kung University*
No.1, Dasyue Rd, East District, Tainan City, Taiwan 701

[c] *Mechanical and Aerospace Engineering Faculty, Bandung Institute of Technology*
Labtek II, 2nd Floor, 10th Ganesha Street, Bandung 40132, Indonesia

Abstract

The non-communicable diseases have become the top cause of global mortality. One of them is stroke, which also become the first cause of disability worldwide. To help rehabilitate the upper extremities function of stroke survivors, a rehabilitation aid robot is developed, also to bridge the gap between patient and medical staff numbers. An end-effector-based rehabilitation robot is one proposed device. In this case, a switched reluctance motor (SRM) can be utilized as the actuator for its simplicity, robustness, high low-speed torque, and low cost. Thus, this paper proposes a design of SRM to be used as the actuator of an end-effector-based wrist rehabilitation robot. The proposed design is made based on the required torque. To extract the outputs, calculation and simulation using finite element magnetic FEMM 4.2 are conducted. The results show that the SRM produces enough torque, according to references. Moreover, rotor tooth width reduction is not preferred, as it increases the negative torque even though it raises the saliency ratio and cuts the mass of the motor.

Keywords: electric motor; end-effector; negative torque; switched reluctance motor; wrist rehabilitation.

I. Introduction

A non-communicable disease (NCD) is a chronic disease that is not transmittable between humans and usually develops slowly over a long period. Data shows that since 1990, the NCDs have been top-ranked in causing global mortality and disability, and their trends are quite concerning [1][2]. Among multiple NCDs, stroke is the most common cause of disability [3]. It also becomes the second most common cause of death, with a 70 % increase in incident strokes, a 43 % increase in death, and a 102 % increase in prevalent strokes [4][5].

One common and serious effect in stroke patients is spasticity of the motor system. Previous references stated a substantial percentage of stroke patients that suffer motor impairment or disabilities in the upper extremities, including shoulders, upper and lower arms,

* Corresponding Author. budi059@brin.go.id (B. Azhari)

https://doi.org/10.55981/j.mev.2024.1109

Received 28 November 2024; revised 17 December 2024; accepted 18 December 2024; available online 31 December 2024;

published 31 December 2024

2088-6985 / 2087-3379 ©2024 The Authors. Published by BRIN Publishing. MEV is Scopus indexed Journal and accredited as Sinta 1 Journal. This is an open access article CC BY-NC-SA license (https://creativecommons.org/licenses/by-nc-sa/4.0/).

How to Cite: B. Azhari *et al*, "Design of switched reluctance motor as actuator in an end-effector-based wrist rehabilitation robot," *Journal of Mechatronics, Electrical Power, and Vehicular Technology*, vol. 15, no. 2, pp. 220-229, Dec. 2024.

elbows, wrist, and fingers. The number ranges between 50 % to 80 % [6][7]. Meanwhile, 34 %-62 % of the patients also have similar problems in the lower extremities, including knees, legs, ankles, and fingers [8]. These conditions should be treated to avoid the risk of declining or diminishing mobility and productivity. In this case, the research is focused on the upper limb, more specifically, the wrist disorder.

To improve or regain motor functions, discipline rehabilitation is a must. Previous researchers showed positive impacts of rehabilitation [9][10], whose form and variety depend on the state of the stroke. So far, direct therapy is still the most practiced rehabilitation. However, the rapid increase in the number of patients causes fear of a widening gap between the number of patients and the medical staff, especially in remote and village areas and in most developing countries. To anticipate this, innovations must be pursued. One of the proposed solutions is using an end-effector-based rehabilitation robot. It is a kind of wearable robot designed to enable patients undergoing rehabilitation by themselves, but it must still be under the supervision of doctors or physiotherapists. Figure 1 displays the example of the applied robot [11].

The end-effector-based robot in this context is a static rehabilitative device. It helps move the upper extremities by holding them from a fixed point. In this case, the end-effector part interacts with the wrist. The patient is positioned in a platform. The affected wrist is then placed into a wearable handler, which is connected to a controlled actuator. This type of robot is considered simple mechanically since its weight and dimension do not affect the patient.

One critical component of the rehabilitation robot is the actuator. Previous designs have implemented several types of actuators. The three most used ones are pneumatic, hydraulic, and electric motors. The pneumatic-based actuators, as implemented in [12][13], are considered compliant, lightweight, and resemble natural muscles with high power-to-weight ratios [14]. However, they are nonlinear, noisy, heavier, and bulkier as they need additional control to make bidirectional motion [15]. Meanwhile, hydraulic actuators can produce higher torque density [16][17], but their designs are quite complex, heavyweight, and have leakage risks [18]. Electric motors are so far widely chosen as actuators due to their simple and compact design, and they are also easier to control with higher accuracy and precision [19][20].

Different previous end-effector-based rehabilitation robots employed electric motors for their actuator. A portable CR2 robot with its reconfigurable design allows its user to train different hand and wrist movements [21]. The post-training assessment showed significant improvement in the range of motion (ROM), including in the wrist. In [22], a 3-DOF upper limb robot was designed and tested, and significant improvement was also recorded in terms of the force of the wrist and forearm. Another reconfigurable 2-DOF wrist rehabilitation device (WreD) was also designed [23]. The WreD comes with an additional mechanical protector and friction reducer to make the user more comfortable. The trajectory tracking shows high accuracy of the device motion. An end-effector upper-limb rehabilitation robot (EULRR) was also designed [24], with a feature of the controller for assist-as-needed (AAN) mode training. The AAN controller provides no assistance when the user's upper limb moves within a certain virtual space but assists when the motion is outside the space. A 2-DOF wrist rehabilitation robot called MOCH was also introduced [25]. It employs a remote center of motion (RCM) based on a parallelogram mechanism, where the center of rotation is outside the robot structure. The structure can reduce the inertia and the risk of motion interference.

Nevertheless, the electric motors utilized above (servo, DC, and BLDC motors) employ permanent magnets (PMs) as the excitation source [21][25]. Although known for its high flux and torque densities, the use of PM is also bound to limited temperature, higher cost, and more complex installation [26]. Moreover, the high flux density-capable rare-earth-based PMs are also known for their material scarcity, unstable supply, and politically influenced price [27][28]. To anticipate these drawbacks, the utilization of non-PM motors needs to be investigated.

Therefore, this paper discusses the use of non-PM motors for an end-effector-based rehabilitation robot. The selected motor is the switched reluctance motor (SRM). Aside from its simple yet robust structure, low cost, and lightweight, the motor is known to have stable torque ability in a wide speed range, relatively high low-speed torque, and low inertia [29][30][31]. In this case,

Figure 1. Example of end-effector-based robot [11].

an SRM design is proposed for the actuator of a 3-DOF wrist rehabilitation robot. The design is made based on the torque requirement of wrist rehabilitation. To obtain and analyze the outputs, calculation and simulation using finite element magnetic software of FEMM 4.2 is performed. The suitability of the motor is then assessed based on its output. The results of the study can become an insight into applying a particular non-PM motor in a rehabilitation robot.

II. Materials and Methods

The SRM design must be suited to its application. Two parameters that are highlighted in a rehabilitation robot are the torque and the range of motion (ROM), as shown in Table 1. According to [32], the wrist torque for normal activities of daily living (ADL) is about 0.35 Nm [32]. For stroke survivors, higher torque needs to be allocated since muscle stiffness should be taken into account. In [33], the generated torque was nearly 1 Nm, produced by a gear-equipped actuator with a gear ratio of 7 (about 0.14 Nm with no gear). Meanwhile, the ROM is used to determine the rotation counts of the motor. There are three motions of the wrist (extension-flexion, abduction-adduction, and pronation supination). Each motion is displayed in Figure 2 and has a specific motion angle range.

A. Design of the end-effector-based robot

The robot comprises a wrist handler, three removable SRMs as the actuator, a separated motor controller, piezoelectric sensors, connecting plates/rods, and a platform (Figure 3). The wrist handler forms a clamper-like platform and is linked to the SRM by using duralumin-made connecting plates. To make users comfortable, the clamp is made of elastic silicon that can be filled with pressured air. Its grip can be set by adjusting the air pressure level, depending on the wrist strength and convenience. Meanwhile, most of the robot structure is made of duralumin, except the rotating gear inside the structure around the wrist for pronation-supination motion, which is made of 3D-printed polyurethane (PU). To ensure the ROM limits are not exceeded, the rotation count of each motor's rotation is limited by setting a separate controller. This controller also manages the speed and torque of the motor. In this paper, however, the controller settings are not detailed. Nevertheless, it has at least three output terminals to control all three motors when being installed at once. To extract the muscle responses, piezoelectric-based sensors are attached to certain spots on the hand. The sensors send the magnetomyography (MMG) signals of the muscle through wires to be processed and analyzed in the controller. The details of the sensor are also excluded from this paper.

Table 1.
Wrist ADL's ROM [30][33].

Wrist motion type	ADL's ROM	ADL's torque
Extension-flexion	52°-45°	0.35 Nm
Abduction-adduction/radial-ulnar	15°-20°	0.35 Nm
Pronation-supination	49°-52°	0.06 Nm

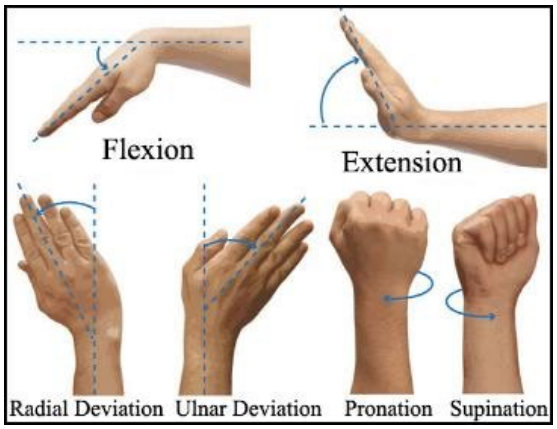

Figure 2. Wrist motion types [34].

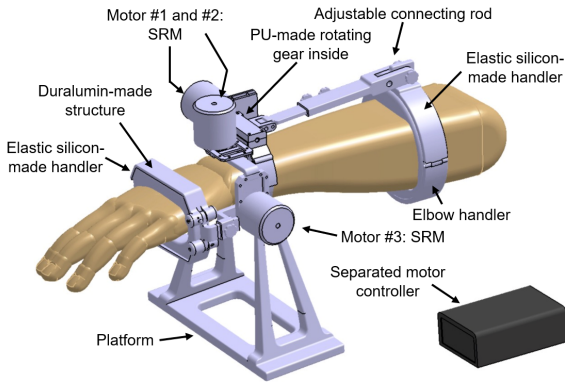

Figure 3. Proposed end-effector-based rehabilitation robot.

Before the rehabilitation process, the clamp is adjusted by manually setting the air pressure. The length of the connecting rod between the wrist and elbow is also regulated. The required torque and motion range are assessed based on the user's requirements read by the sensors, and the controller is set accordingly. The motor is then turned on and its rotation activates the wrist movement. During the rehabilitation process, the sensors keep extracting the MMG signals of the muscles to adjust the motor controller continuously.

B. Design of the switched reluctance motor (SRM)

Figure 4 displays the proposed SRM design, while Table 2 shows the parameters and complete dimensions of the SRM parts. The motor consists of an inner rotor

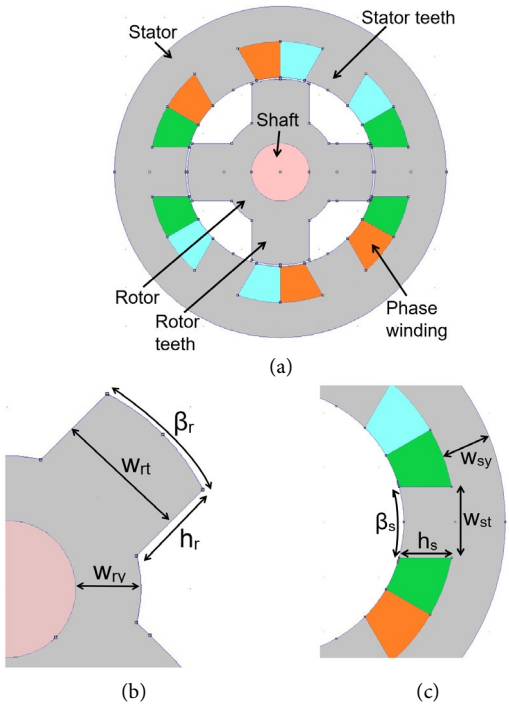

Figure 4. (a) The proposed SRM design; (b) Rotor; (c) stator.

and an outer stator. Both parts are made of silicon iron sheets laminated in an in-plane direction with a factor of 0.98. The shaft is coupled with the connecting plates, which link to the wrist handler.

The stator Figure 5 has six teeth with double-layer concentrated windings wound on the slots between them Figure 5(a), driven by a 3-phase inverter, as shown in Figure 5(b). On the other hand, the rotor has four teeth whose ends make curves with a larger angle than the stators'. The air gap between the rotor and stator is 0.5 mm.

One important part of an SRM is the teeth of both the stator and rotor. Their width affects the magnetic flux path, especially in unaligned positions (Figure 6). The magnitude will affect the inductance difference, which will lead to torque generation. Furthermore, both parts also affect the resulting SRM mass. Meanwhile, other parts, such as the tooth height and

Table 2.
Parameter and Dimension of the SRM.

Part symbol	Unit	Value
Rated speed, n_s	rpm	84
Peak phase current, $I_{ph(pk)}$	A	2.2
Terminal voltage, V_{dc}	V	12
Stator outer diameter, D_o	mm	86.8
Stator inner diameter, D	mm	50
Stator yoke thickness, w_{sy}	mm	9.1
Stator tooth height, h_s	mm	9.3
Stator tooth width, w_{st}	mm	12.9
Stator tooth arc, β_s	deg (°)	30
Rotor yoke thickness, w_{ry}	mm	7.1
Rotor tooth height, h_r	mm	9.4
Rotor tooth width, w_{rt}	mm	14.8
Rotor tooth arc, β_r	deg (°)	36
Shaft diameter, D_{sh}	mm	15

yoke thickness of the stator and rotor, also shape the mass and influence the magnetic flux. However, the flux is affected under both unaligned and aligned positions. Thus, the inductance difference does not significantly change.

The width of each tooth can be calculated using the equation (1), equation (2), equation (3), equation (4).

$$\beta_s = \xi_s \frac{2\pi}{n_s}, \quad (1)$$

$$\beta_r = \xi_r \frac{2\pi}{n_r}, \quad (2)$$

$$w_{rt} = 2\left(\frac{D}{2} - g\right) sin\frac{\beta_r}{2} \quad (3)$$

$$w_{st} = D\, sin\frac{\beta_s}{2} \quad (4)$$

where β_s and β_r are the tooth arc of the stator and rotor, respectively (rad), ξ_s and ξ_r are the tooth arc coefficient of the stator and rotor, and n_s and n_r are the number of stator and rotor teeth. Moreover, w_{rt} and w_{st} are the tooth width of the stator and rotor (m), D is the stator inner diameter (m), and g is the air gap (m).

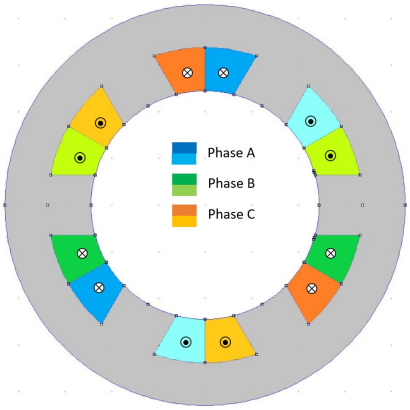

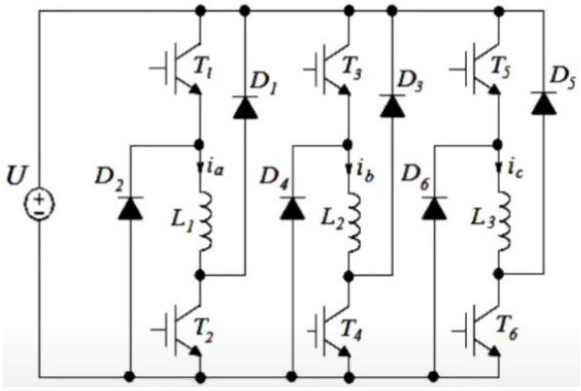

Figure 5. (a) Winding scheme of the proposed SRM; (b) inverter scheme of the SRM.

The tooth height also affects the reluctance, hence the magnetic flux. The height of the stator and rotor teeth can be found using the equation (5), equation (6), equation (7).

$$h_{rt} = \frac{D}{2} - g - \frac{D_{sh}}{2} - w_{ry} \quad (5)$$

$$h_{st} = d_c + h_o \quad (6)$$

$$d_c = \frac{\sqrt{(\pi D + 2\pi h_o - w_{st} n_s)^2 - 8\pi n_s k_f N_{tc} A_{cw}} - (\pi D + 2\pi h_o - w_{st} n_s)}{2\pi} \quad (7)$$

where D_{sh} is shaft diameter (m), w_{ry} is rotor yoke thickness (m), h_o is winding-stator tooth gap (m), and k_f is the fill factor of the winding. Furthermore, N_{tc} is the number of winding turns per coil, and A_{cw} is the surface area of the wire (m^2). The wire surface area is related to the maximum allowed stator current.

C. Calculation and simulation of the SRM outputs

After completing the design, the output of the SRM needs to be tested in terms of compatibility with the required value. To extract some outputs, simulation is performed by using the finite element method (FEM) magnetostatic mode of FEMM 4.2 [35]. In this mode, the solution for magnetic field (H, in A/m) and flux density (B, in T) can be approached by finding magnetic vector potential (A, in Vs/m) that satisfies the following equations.

$$\nabla \times H = J; \nabla \cdot B = 0; \mu H = B \quad (8)$$

The vector potential A is defined by the equation below.

$$\nabla \times A = B. \quad (9)$$

The current flows sequentially to the phase windings, causing the rotor to rotate. Under a certain rotor position, instantaneous inductance can be calculated from magnetic field energy (W_m, in J), that is obtained from the simulation.

$$L(\theta, i) = \frac{2W_m}{i(\theta)^2} = \frac{\int A \cdot J dV}{i(\theta)^2} \quad (10)$$

In SRM, the difference between aligned inductance (L_d) and unaligned inductance (L_q) (Figure 6), both in Henry, plays a significant role in determining the output power (P_o) and torque (T_e). They can be calculated using the equation (11), equation (12), equation (13) [36][37].

$$\varepsilon = \frac{L_d}{L_q}, \quad (11)$$

$$P_o = \frac{\pi^2}{2}\left(1 - \frac{1}{\varepsilon}\right)\frac{\beta_s}{\theta_c} B_o A_c D^2 l_{st} n, \quad (12)$$

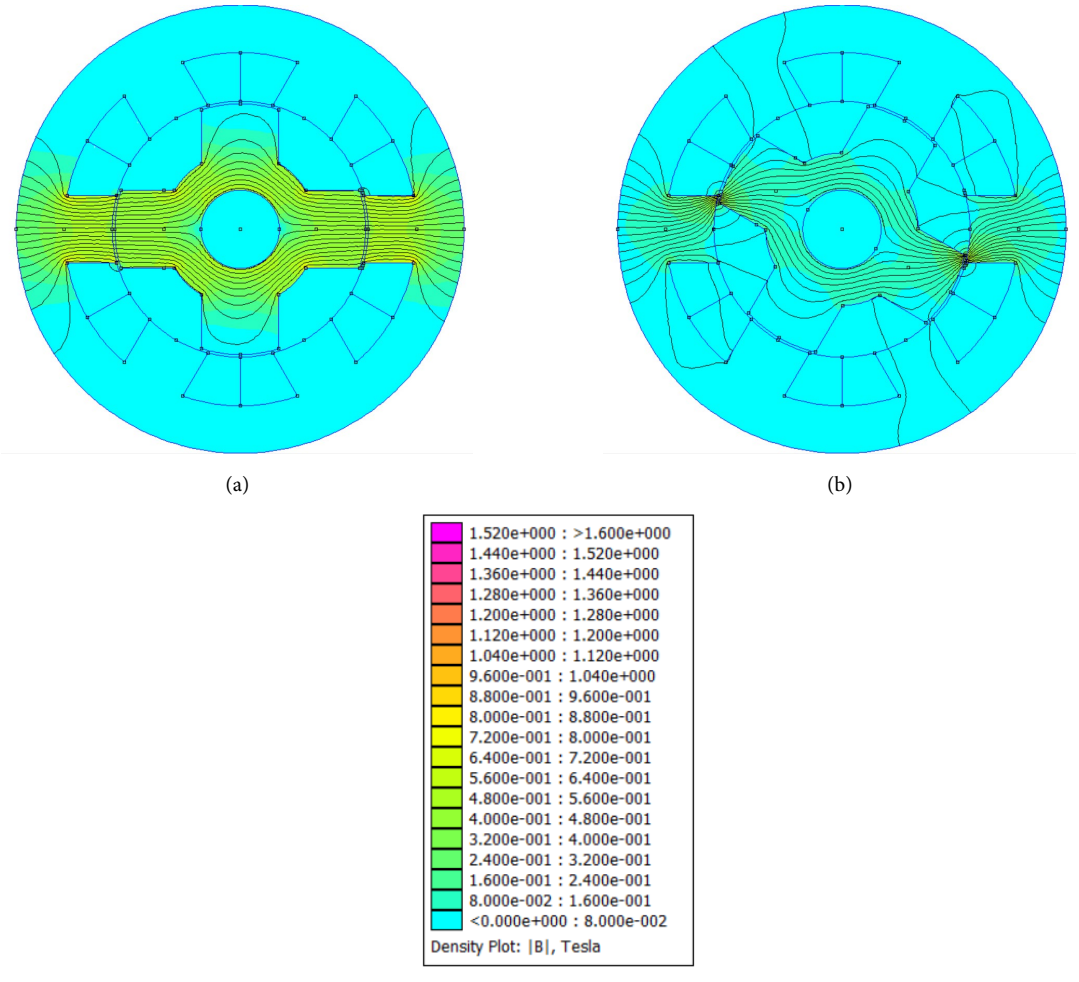

Figure 6. Magnetic flux: (a)aligned; (b) unaligned positions.

Table 3.
Results of unaligned and aligned inductances from different rotor tooth width.

Rotor tooth width, w_{rt} (mm)	Air gap flux density (T)	L_q (H)	L_d (H)	Saliency ratio (ε)
14.8	0.162	0.0136	0.1110	8.134
14.0	0.140	0.0131	0.1104	8.407
13.0	0.099	0.0125	0.1092	8.715

$$T_e = \frac{1}{2} i^2 \left(\frac{dL(\theta,i)}{d\theta}\right). \quad (13)$$

where ε is the saliency ratio, B_o and A_c are the magnetic loading (T) and electrical loading (A/m), respectively, l_{st} is the SRM axial length (m), θ_c is the conducting phase (rad), n is the rotating speed (rps), i is phase current (A), and θ is position angle (rad).

The mass of the motor active part (m, in kg) is as equation (14).

$$m = \left(\pi \frac{\left(D_o{}^2 - (D_o - 2w_{sy})^2\right)}{4} + n_s w_{st} h_s\right) l_{st} \rho_{st} + \left(\pi \frac{\left((D_{sh} + 2w_{ry})^2 + D_{sh}{}^2\right)}{4} + n_r w_{rt} h_r\right) l_{rt} \rho_{rt} + n_s N_{tc} A_{cw} t_{lav} \rho_w. \quad (14)$$

where ρ_{st}, ρ_{rt}, and ρ_w are the mass density of stator, rotor, and winding (kg/m^3) successively, A_{cw} is copper wire cross-section area (m^2), and t_{lav} is winding mean turn length (m).

III. Results and Discussions

In analyzing the proposed SRM design, some important parameters are varied and analyzed. First, the impact of rotor tooth width modification on the SRM output is investigated. Next, the impact of the stator current changes on the SRM output is also assessed. From the assessment, the optimum design is chosen, and its suitability for the rehabilitation robot is explored. Furthermore, the optimum design criteria can be elaborated for the next optimization project.

A. Effect of rotor tooth width

The inductance plays an important role in determining the output. It is related to the magnetic flux generated when an input current is injected and affects the output torque. The rotation of the rotor results in unaligned and aligned (Figure 6) inductances. Both parameters are affected by the design of stator and rotor teeth. The rotor tooth width and the rotor yoke thickness affect the air gap during unaligned positions. A larger gap results in a longer distance between the stator teeth of an active phase and the nearest rotor teeth, making a higher reluctance. Higher reluctance results in smaller inductance. The rotor tooth width also determines the surface area of the rotor edge during the aligned position, which negatively affects the reluctance and positively the inductance. The air gap flux densities and inductances for different rotor tooth widths but the same phase currents in both aligned and unaligned positions are tabulated in Table 3.

The magnetic flux decreases as the rotor tooth width decreases. As the flux decreases, the phase inductance also drops. However, the decrease in the tooth width increases the saliency ratio, which can affect the output power positively. Therefore, the reduction of the rotor tooth width has a positive impact.

The next factor to be noticed is the pattern of the phase inductance. When the rotor rotates, the inductance of a certain phase increases from its unaligned value (L_q) to its aligned value (L_d). When the current is at its peak for a certain moment, the inductance rises because the rotor tooth position is getting more aligned with the stator tooth. When all stator tooth surfaces are facing the rotor tooth surface, the inductance reaches its peak and stays so until the unalignment starts. The moment phase inductance reaches the peak, the next negative trend should be minimized. According to (13), the negative trend results in negative torque, which negatively impacts the rotor movement. In this case, the stator and rotor teeth play an important role.

Figure 7 displays the phase inductances under moving position and respective phase current changes for several rotor tooth width values. Position 0° is the unaligned position, and position 37.5° is the starting position when the stator tooth surface entirely faces the rotor tooth surface. For a rotor tooth width of 13 mm, the peak inductance decreases quite sharply and quickly. This decreasing slope is reduced with the increase of the rotor tooth width. For a tooth width of 14.8 mm, the inductance still decreases but on a smaller slope. This trend affects the resulting torques.

Figure 8 presents the output torque of the SRM with different tooth widths. The output torque from different rotor tooth widths resulting similar output torque. As the torque is generated from the change in inductance, the value can be tracked from the inductance graph (Figure 7). The inductance from different tooth widths has a similar positive gradient or slope. Therefore, the change in the rotor teeth does not affect the torque capacity of the SRM.

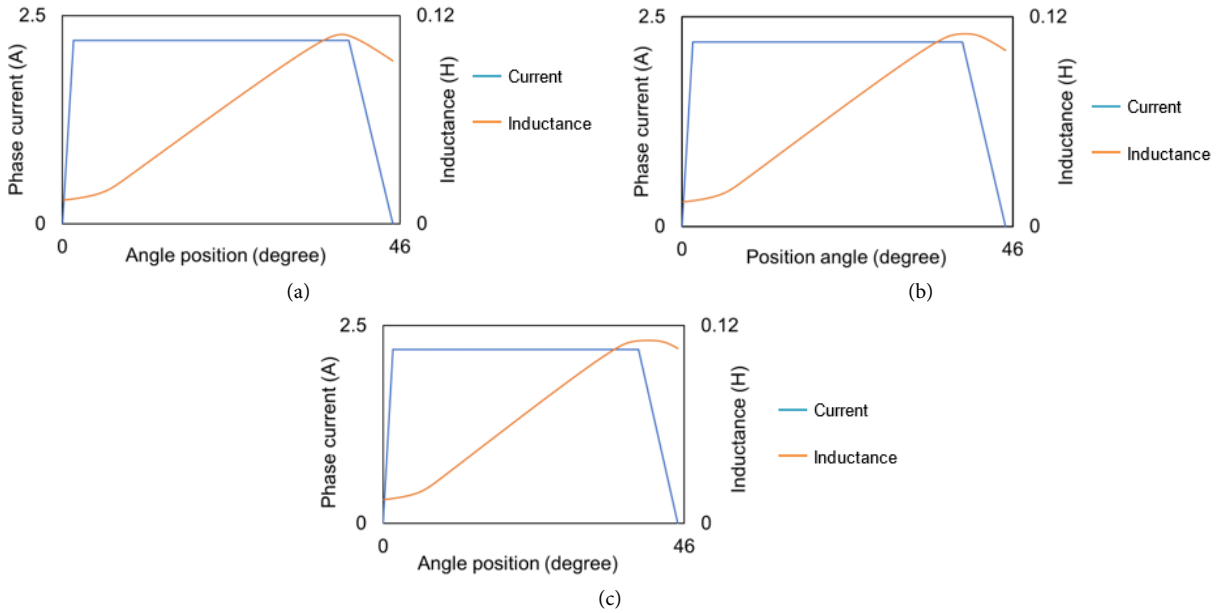

Figure 7. Phase inductance graphs under moving position and respective current for rotor tooth width of (a) 13 mm; (b) 14 mm; (c) 14.8 mm.

On the other hand, the different tooth widths bring different negative torques. Related to the inductance graph pattern, the negative torque generated is directly proportional to the negative gradient of the peak inductance. This trend is related to the inductance graphs. In this case, the rotor tooth width of 14.8 mm produces the minimum negative torque, just as it produces the minimum inductance's negative slope. From the aspect of inductance and resulting negative torque, the decrease of the rotor tooth width has a negative impact.

The other important aspect is mass. Although not crucial in an end-effector-based robot, it still matters to note. The decrease of the rotor tooth width certainly reduces the mass, for other parts are kept the same. Therefore, the reduction impacts positively. Table 4 shows the comparison between the mass for different rotor tooth widths. In this case, the mass is represented by the active parts (rotor, stator, winding).

From the aforementioned impacts, the decrease of the rotor tooth width affects both positively (on the saliency ratio and mass) and negatively (on the negative torque). For the end-effector-based rehabilitation robot, the negative torques play a more important role than other parameters. They affect the rotor motion, which directly influences the wrist motion during the rehabilitation process. Meanwhile, the mass in an end-effector robot is absorbed by the robot's platform and does not affect the user. Therefore, the proposed SRM, as listed in Figure 4 and Table 2, is adopted, where the rotor tooth width is 14.8 mm. Figure 8 and Table 4 show that the SRM can produce an output torque of 0.415 Nm. It has exceeded the ADL value in [32] and the output torque of the actuator without gear in [33]. To increase the output torque for anticipating a higher degree of muscle stiffness in certain stroke patients, a gearbox transmission with a relatively small gear ratio can be added.

Table 4.
Active part mass comparison for different rotor tooth width.

Parameter	Unit
14.8	2.222
14.0	2.205
13.0	2.173

B. Effect of stator current

Furthermore, the output torque is also affected by the input current. The current represents the power injected into the motor. Figure 9 shows the torque graphs under different peak phase currents. The graphs help understand how much the tolerance of current reduction is to generate the minimum torque. It is found that while the peak phase current decreases with a constant difference, the reduction rate of the torque increase in every current reduction. Hence, for this design, the peak phase current is kept according to Table 2, which is 2.2 A. Nonetheless, the larger current draws a larger copper loss. It is inevitable that non-PM motors will replace the PM-based ones. Because it needs to compensate for the amount of magnetic flux that cannot be produced by permanent magnets. It is then required to maintain stator current as efficiently as possible to maximize the generated torque.

C. Suitability of the actuator and next project plan

Based on the required torque in the collected references, the proposed SRM design can fulfill the requirement. Nevertheless, the SRM also produces a

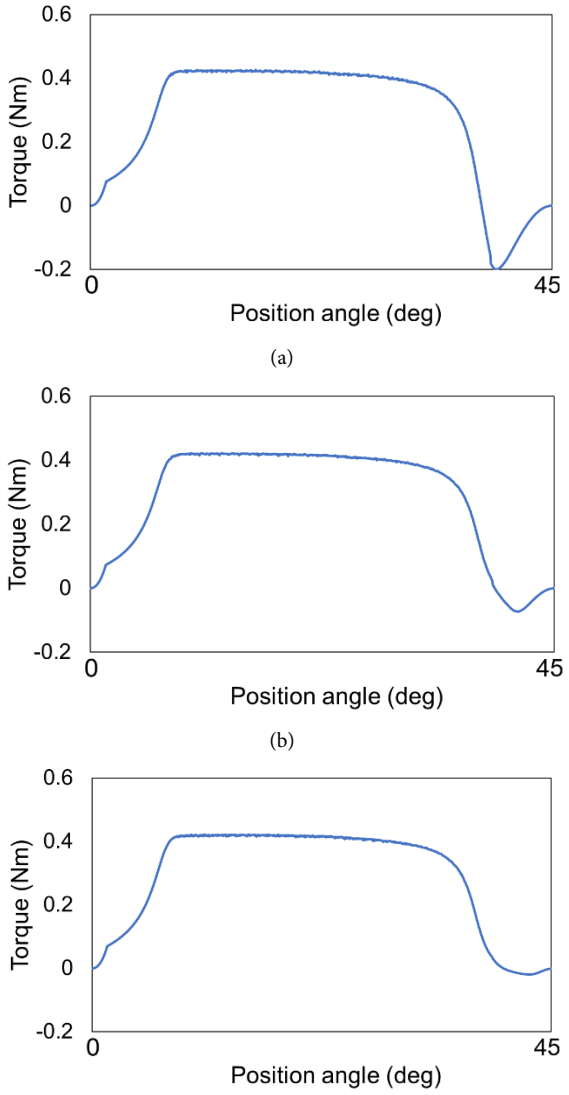

Figure 8. Output torque graphs under moving position and respective current for rotor tooth width of (a) 13 mm, (b) 14 mm, (c) 14.8 mm.

high torque ripple, which still needs to be addressed. The ripple, along with negative torque, can result in motion disturbance during rehabilitation. In [38], multiple efforts are taken to minimize the torque ripple, both from the geometry and control aspects. Those steps can be taken in future research.

Based on this investigation, design optimization can also be performed using the criteria obtained. The negative torque should be minimized while the saliency ratio is maximized. Other aspects, including mass, volume, and efficiency, can also be included to be optimized. Additional features such as back-drivability and motor response to load change can also be explored.

Furthermore, Figure 10 displays the manufacturing drawing plan of the SR motor based on the optimum design in this paper. The rotor sheets are pressed and bolted using four M3 bolts. Meanwhile, the stator sheets are pressed and held by the SRM casing. Furthermore, the shaft is held by two 61800 bearings at

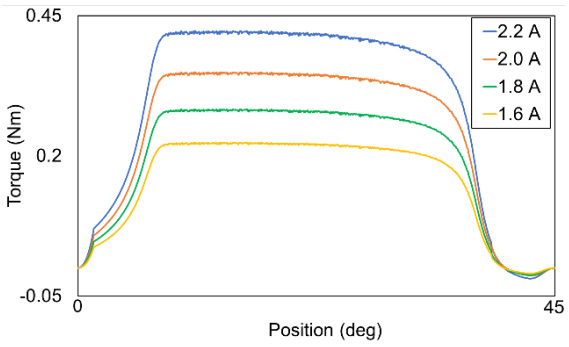

Figure 9. Output torque graphs under different phase currents.

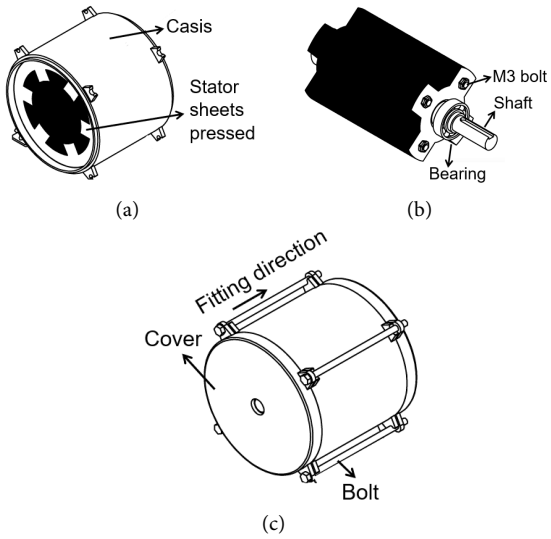

Figure 10. (a) Manufacturing drawing of stator; (b) rotor; (c) overall SR motor.

both ends to regulate its rotation. The SRM motor is fitted perpendicularly into the rehabilitation platform using four bolts and flanges outside the casis.

IV. Conclusion

This paper proposes a non-PM motor as an actuator in an end-effector-based rehabilitation to help wrist rehabilitation. A switched reluctance motor (SRM) is selected and designed based on the torque requirement of wrist rehabilitation. Different tooth widths and stator currents are tested. The results show that the decrease of the rotor tooth width affects both positively (on the saliency ratio and mass) and negatively (on the rise of negative torque). Meanwhile, the current is directly proportional to the output torque. Based on the results, an optimum design is selected to minimize the negative torque while maximizing the output torque. Using the optimum design, the SRM can produce torque that exceeds the references' magnitude. In the next project, torque ripple minimization can be performed while optimizing the geometry to minimize the mass and negative torque and maximize the saliency ratio.

Acknowledgements

The authors would like to thank the Research Organization for Health (Organisasi Riset Kesehatan), National Research and Innovation Agency of the Republic of Indonesia (BRIN), for this research is supported through funding under the Research Program (Rumah Program) of Prototype of Medical Devices (Purwarupa Alat Kesehatan) number 6/III.9/HK/2024, year 2024.

Declarations

Author contribution

B. Azhari: writing-original draft, writing-review & editing, conceptualization, formal analysis, investigation, validation, visualization. **M.F. Hikmawan** and **A.S. Nugraha**: review & editing, validation, supervision. **E. Yazid**: review & editing, supervision, funding acquisition, **C.H.A.H.B. Baskoro**: validation, review & editing. **Rahmat**: software, visualization. **A.N. Pakha** and **M.L. Ramadiansyah**: review & editing

Funding statement

This research did not receive any specific grant from funding agencies in the public, commercial, or not-for-profit sectors.

Competing interest

The authors declare that they have no known competing financial interests or personal relationships that could have appeared to influence the work reported in this paper.

Additional information

Reprints and permission: information is available at https://mev.brin.go.id/.

Publisher's Note: National Research and Innovation Agency (BRIN) remains neutral with regard to jurisdictional claims in published maps and institutional affiliations.

References

[1] T. Vos *et al.*, "Global burden of 369 diseases and injuries in 204 countries and territories, 1990–2019: a systematic analysis for the Global Burden of Disease Study 2019," *The Lancet*, vol. 396, no. 10258, pp. 1204–1222, Oct. 2020.

[2] World Health Organization, "Non-communicable diseases country profiles 2018". *Geneva: World Health Organization*, 2018. [Online] [Accessed: Jul. 10, 2024].

[3] World Stroke Day 2022. *Geneva: World Health Organization*, 29 October 2022. [Online] [Accessed: Jul. 10, 2024].

[4] "Corrigendum to: World Stroke Organization (WSO): Global Stroke Fact Sheet 2022," *International Journal of Stroke*, vol. 17, no. 4, pp. 478–478, Apr. 2022.

[5] L. Andriani, "Dominasi penyakit tidak menular dan pola makan yang tidak sehat," *Pros Sem Nas Masy Biodiv Indon* 2020. vol. 6, no. 1, pp. 649–652, jun. 2020 [Online] [Accessed: Jul. 10, 2024]

[6] E. S. Lawrence *et al.*, "Estimates of the Prevalence of Acute Stroke Impairments and Disability in a Multiethnic Population," *Stroke*, vol. 32, no. 6, pp. 1279–1284, Jun. 2001.

[7] H. C. Persson, M. Alt Murphy, A. Danielsson, Å. Lundgren-Nilsson, and K. S. Sunnerhagen, "A cohort study investigating a simple, early assessment to predict upper extremity function after stroke - a part of the SALGOT study," *BMC Neurol*, vol. 15, no. 1, p. 92, Dec. 2015.

[8] V. Darak and S. Karthikbabu, "Lower limb motor function and hip muscle weakness in stroke survivors and their relationship with pelvic tilt, weight-bearing asymmetry, and gait speed: A cross-sectional study," *CJN*, Jun. 2020.

[9] S. Hussain, P. K. Jamwal, P. Van Vliet, and M. H. Ghayesh, "State-of-the-Art Robotic Devices for Wrist Rehabilitation: Design and Control Aspects," *IEEE Trans. Human-Mach. Syst.*, vol. 50, no. 5, pp. 361–372, Oct. 2020.

[10] S. Tenberg *et al.*, "Comparative Effectiveness of Upper Limb Exercise Interventions in Individuals With Stroke: A Network Meta-Analysis," *Stroke*, vol. 54, no. 7, pp. 1839–1853, Jul. 2023.

[11] T. Anne, "Robotic therapy helps stroke patients regain function," *MIT News website*, [Online]. [Accessed: Jul 20, 2024].

[12] T. Ridremont *et al.*, "Pneumatically Actuated Soft Robotic Hand and Wrist Exoskeleton for Motion Assistance in Rehabilitation," *Actuators*, vol. 13, no. 5, p. 180, May 2024.

[13] Y. Wang and Q. Xu, "Design and testing of a soft parallel robot based on pneumatic artificial muscles for wrist rehabilitation," *Sci Rep*, vol. 11, no. 1, p. 1273, Jan. 2021.

[14] M. Haghshenas-Jaryani, R. M. Patterson, N. Bugnariu, and M. B. J. Wijesundara, "A pilot study on the design and validation of a hybrid exoskeleton robotic device for hand rehabilitation," *Journal of Hand Therapy*, vol. 33, no. 2, pp. 198–208, Apr. 2020.

[15] F. Hussain, R. Goecke, and M. Mohammadian, "Exoskeleton robots for lower limb assistance: A review of materials, actuation, and manufacturing methods," *Proc Inst Mech Eng H*, vol. 235, no. 12, pp. 1375–1385, Dec. 2021.

[16] M. A. Gull, S. Bai, and T. Bak, "A Review on Design of Upper Limb Exoskeletons," *Robotics*, vol. 9, no. 1, p. 16, Mar. 2020.

[17] A. Otten, C. Voort, A. Stienen, R. Aarts, E. Van Asseldonk, and H. Van Der Kooij, "LIMPACT:A Hydraulically Powered Self-Aligning Upper Limb Exoskeleton," *IEEE/ASME Trans. Mechatron.*, vol. 20, no. 5, pp. 2285–2298, Oct. 2015.

[18] M. Tiboni, A. Borboni, F. Vérité, C. Bregoli, and C. Amici, "Sensors and Actuation Technologies in Exoskeletons: A Review," *Sensors,* vol. 22, no. 3, p. 884, Jan. 2022.

[19] A. J. Veale and S. Q. Xie, "Towards compliant and wearable robotic orthoses: A review of current and emerging actuator technologies," *Medical Engineering & Physics*, vol. 38, no. 4, pp. 317–325, Apr. 2016.

[20] S. Kumar *et al.*, "Modular Design and Decentralized Control of the Recupera Exoskeleton for Stroke Rehabilitation," *Applied Sciences*, vol. 9, no. 4, p. 626, Feb. 2019.

[21] K. X. Khor *et al.*, "Portable and Reconfigurable Wrist Robot Improves Hand Function for Post-Stroke Subjects," *IEEE Trans. Neural Syst. Rehabil. Eng.*, vol. 25, no. 10, pp. 1864–1873, Oct. 2017.

[22] E. Akdoğan, M. E. Aktan, A. T. Koru, M. Selçuk Arslan, M. Atlıhan, and B. Kuran, "Hybrid impedance control of a robot manipulator for wrist and forearm rehabilitation: Performance analysis and clinical results," *Mechatronics*, vol. 49, pp. 77–91, Feb. 2018.

[23] D. Xu, M. Zhang, H. Xu, J. Fu, X. Li, and S. Q. Xie, "Interactive Compliance Control of a Wrist Rehabilitation Device (WR e D) with Enhanced Training Safety," *Journal of Healthcare Engineering*, vol. 2019, pp. 1–10, Feb. 2019.

[24] L. Zhang, S. Guo, and Q. Sun, "Development and Assist-As-Needed Control of an End-Effector Upper Limb Rehabilitation Robot," *Applied Sciences*, vol. 10, no. 19, p. 6684, Sep. 2020.

[25] A. Molaei, N. A. Foomany, M. Parsapour, and J. Dargahi, "A portable low-cost 3D-printed wrist rehabilitation robot: Design and development," *Mechanism and Machine Theory*, vol. 171, p. 104719, May 2022.

[26] S. Han, K. Diao, and X. Sun, "Overview of multi-phase switched reluctance motor drives for electric vehicles," *Advances in Mechanical Engineering*, vol. 13, no. 9, p. 16878140211045195, Sep. 2021

[27] S. Zheng, X. Zhu, Z. Xiang, L. Xu, L. Zhang, and C. H. T. Lee, "Technology trends, challenges, and opportunities of reduced-rare-earth PM motor for modern electric vehicles," *Green Energy and Intelligent Transportation*, vol. 1, no. 1, p. 100012, Jun. 2022.

[28] P. C.-K. Luk, H. A. Abdulrahem, and B. Xia, "Low-cost high-performance ferrite permanent magnet machines in EV applications: A comprehensive review," *eTransportation*, vol. 6, p. 100080, Nov. 2020.

[29] F. Kucuk and T. Nakamura, "Low-Cost Permanent Magnet-Assisted Switched Reluctance Motor for Adjustable Speed Drive Applications," *IEEJ Transactions Elec Engng,* vol. 15, no. 8, pp. 1213–1218, Aug. 2020.

[30] S. Yang et al., "A novel wrist rehabilitation exoskeleton using 3D-printed multi-segment mechanism," in 2021 *43rd Annual International Conference of the IEEE Engineering in Medicine & Biology Society (EMBC), Mexico: IEEE,* Nov. 2021, pp. 4769–4772.

[31] Y. Lan et al., "Switched Reluctance Motors and Drive Systems for Electric Vehicle Powertrains: State of the Art Analysis and Future Trends," *Energies*, vol. 14, no. 8, p. 2079, Apr. 2021.

[32] N. Nikafrooz, M. J. Mahjoob, and M. Ali Tofigh, "Design, Modeling, and Fabrication of a 3-DOF Wrist Rehabilitation Robot," in 2018 *6th RSI International Conference on Robotics and Mechatronics (IcRoM), Tehran, Iran: IEEE,* Oct. 2018, pp. 34–39.

[33] A. U. Pehlivan, F. Sergi, A. Erwin, N. Yozbatiran, G. E. Francisco, and M. K. O'Malley, "Design and validation of the RiceWrist-S exoskeleton for robotic rehabilitation after incomplete spinal cord injury," *Robotica*, vol. 32, no. 8, pp. 1415–1431, Dec. 2014.

[34] L. Arianna, "De Quervain's Disease/Tenosynovitis" Morphopedics. [Online]. [Accessed: Jul 20, 2024].

[35] D. C. Meeker, "Finite Element Method Magnetics, Version 4.2 (28Feb2018 Build)" *Finite Element Method Magnetics*, [Online]. [Accessed: Jul 20, 2024]

[36] Krishnan, R., "Switched Reluctance Motor Drives: Modeling, Simulation, Analysis, Design, and Applications (1st ed.)". *CRC Press*. 2001.

[37] Y. Zhang, L. Chen, Z. Wang, and E. Hou, "Speed Control of Switched Reluctance Motor Based on Regulation Region of Switching Angle," *Energies*, vol. 15, no. 16, p. 5782, Aug. 2022.

[38] Y. Lan *et al.*, "Switched Reluctance Motors and Drive Systems for Electric Vehicle Powertrains: State of the Art Analysis and Future Trends," *Energies*, vol. 14, no. 8, p. 2079, Apr. 2021.